THE ASTROPHYSICAL JOURNAL, 451:176–187, 1995 September 20

H II REGIONS IN FOUR GALAXIES IN AND NEAR THE LOCAL GROUP

PAUL HODGE[1] AND BRYAN W. MILLER[1,2]
Astronomy Department, University of Washington, Seattle, WA 98195
Received 1994 November 28; accepted 1995 March 21

ABSTRACT

We present identifications, fluxes, and sizes for H II regions in three galaxies that are in or near the Local Group: WLM, UGC A86, and EGB 0427+63. A deep search for H II regions in a fourth galaxy, LGS 3, produced a negative result. Our results for UGC A86 indicate that, contrary to a previous suggestion, it is a single galaxy. Its disjointed appearance in broadband images apparently is caused by the presence of several star-forming regions of different ages. Our data, together with other information about it, especially its radial velocity, also suggest that this object is beyond the limits of the Local Group.

The H II regions of the three galaxies in which they were detected show normal luminosity functions that fit power laws and normal size distributions that are reasonably well fitted by an exponential function. The calculated star formation rates range from zero for LGS 3 to 0.014 $M_\odot$ yr^{-1} for UGC A86.

Emission-line spectra of seven H II regions in the three galaxies allow abundances to be determined. We find that all are low in heavy elements, with mean values for O/H of approximately 7% solar.

Subject headings: galaxies: stellar content — galaxies: structure — H II regions — ISM: abundances — Local Group — stars: formation

1. INTRODUCTION

This paper presents photometric and spectroscopic data for four galaxies that are members of the Local Group or have been candidates for membership. It continues a series of such studies that has as its intention the production of a uniform set of H II region data for all Local Group members, which we plan to use to study the star formation process and its evolution in the nearly complete sample of galaxies provided by the Local Group. An analysis of this kind is given in Hodge (1994), which references our earlier papers.

WLM.—The WLM galaxy is a Local Group irregular, discovered independently by Wolf, Lundmark, & Mellotte (Sandage & Carlson 1985). It has a low surface brightness and a typical irregular galaxy structure (Ables & Ables 1977) and is rich in H I (Richter, Tammann, & Huchtmeier 1987). Photometry of its resolved stellar population (Sandage & Carlson 1985; Ferraro et al. 1989) indicates an irregular pattern of recent star formation. Its heavy element abundance is 7% solar (Skillman, Terlevich, & Melnick 1989). Photometry of a number of variable stars has revealed at least 15 Cepheids (Sandage & Carlson 1985). In this paper we adopt a distance modulus of $(m - M)_{AB} = 25.0$ and a reddening of $E(B-V) = 0.02$.

EGB 0427+63.—The small irregular galaxy known as EGB 0427+63 (=UGC A92) was cataloged as a possible planetary nebula by Ellis, Grayson, & Bond (1984). Hoessel, Saha, & Danielson (1988) identified it as a galaxy and tentatively placed it at a distance of 800 kpc. In this paper we adopt this value, which, together with the reddening they adopted ($A_r = 0.57$: Burstein & Heiles 1984; Schneider, Gunn, & Hoessel 1983), leads to a foreground reddening of $E(B-V) = 0.25$ and a tentative distance modulus of $(m - M)_0 = 24.5$. We consider this distance modulus a lower limit, with values as high as 28 considered possible.

UGC A86.—UGC A86 (=VII Zw 009) is a dwarf galaxy studied photometrically by Saha & Hoessel (1991), who suggested that it might be a Local Group member. They also suggested, on the basis of its broadband morphology, that it might be two galaxies accidentally nearly superposed. Regarding its distance, however, Kraan-Korteweg & Tammann (1979) place it beyond the Local Group, assigning it to the IC 342 group. Based on its position and radial velocity, van den Bergh (1994) also excludes it from the Local Group. Richter et al. (1991) have carried out photographic photometry and have concluded that it is a single object with two main star-forming regions, the southern one being the brighter and bluer. The *IRAS* source 3550+665 seems to correspond in position to UGC A86, and Richter et al. (1991) believe that it indicates the presence of a considerable extinction in the galaxy's star-forming regions.

While Saha & Hoessel (1991) suggest a very small distance modulus, $(m - M)_0 = 24$, an association with IC 342 would indicate a distance of 4.7 Mpc (Kraan-Korteweg & Tammann 1976). Karachentsev & Tikhonov (1993) give a distance of 1.86 Mpc, based on a brightest star criterion. Miller and Hodge (1992), using the marginally reliable H II region size scale length criterion (Hodge 1983), derived a distance of 2.1 ± 0.5 Mpc. Taking a mean of these values leads to an estimate of 2.3 (±1.6) Mpc, which we round off to 2 Mpc.

The foreground reddening is also very uncertain. The H I maps in this part of the sky shown widely variable densities. Based on the Burstein & Heiles graphs, the value of $E(B-V)$ for this position is 0.61, with a large uncertainty because of the variability over small scales. On the other hand, use of a cosecant law gives smaller values, averaging about 0.20, while Richter et al. (1991) argue that it may be much larger, based on the *IRAS* source. The large uncertainty in distance combines with this uncertainty in reddening to leave the absolute characteristics of this galaxy very uncertain. For this paper, we adopt a distance of 2 Mpc and a mean reddening of $E(B-V) = 0.65$.

[1] Visiting astronomers, Kitt Peak National Observatory, which is operated by AURA, Inc., under contract to the National Science Foundation.
[2] Present address: Carnegie Institution of Washington, 5241 Broad Branch Road, NW, Washington, DC 20015.

TABLE 1

ADOPTED PROPERTIES OF THE SAMPLE

Galaxy	$E(B-V)$ (Foreground)	B_T°	$(B-V)_T^\circ$	$(m-M)_0$	M_B
WLM	0.02	10.58	+0.31	25.0	−14.4
EGB 0427+63.....	0.25	...	...	24.5	...
UGC A86	0.65	12.7	...	26.5	−13.8
LGS 3	0.08	15.5	...	24.4	9.2

[a] Data sources are as follows: *Reddenings*: see text. *Magnitudes and colors*: WLM and LGS 3, de Vaucouleurs et al. 1991; UGC A86, Richter et al. (1991). *Distances*: see text.

LGS 3.—The very faint Local Group galaxy LGS 3 (Thuan & Martin 1979) is an anomalous object, with a globular cluster–like color-magnitude diagram (Cook & Olszewski 1989) and a significant though small H I content (Lo, Sargent, & Young 1993).

A summary table providing the adopted values of the basic properties of the galaxies is given in Table 1.

2. OBSERVATIONS

The observational material for this paper was obtained at the Kitt Peak National Observatory. The Hα narrow-band images were obtained on 1991 December 14 and 15 with the 0.9 m telescope. The CCD images were exposed through a 38 Å half-power bandwidth Hα interference filter for the on-line images and a 270 Å bandwidth filter centered on 6092 Å for the continuum images. Observations of Feige 34 provided absolute calibration.

Reductions of the CCD images followed the procedures detailed in Appendix A of our paper on the M81 Group dwarfs (Miller & Hodge 1994); they involved determining extinction, folding in the filter response functions, matching the point-spread functions, and including the standard star spectra.

The spectroscopic data were obtained on 1993 September 17–19 using the Gold Spectrograph and a Ford 1024 × 3072 pixel CCD on the KPNO 2.1 m telescope. Grating 240 was used to provide wavelength coverage from 3100 Å to 7600 Å with a resolution of ∼6 Å. A WG345 filter was used to minimize light leaks. All observations were obtained through thin clouds, and so absolute calibration was not possible. Relative calibration was attained through observations of intensified Reticon scanner (IRS) standard stars Feige 34, BD +28 4211, and Hiltner 102, which were observed frequently throughout the run. The 4″ wide slit was positioned on the H II regions by means of off-sets from nearby stars. A 10″ wide slit was used for the standard stars. Usable spectra were obtained for two H II regions in EGB 0427+63, two in UGC A86, and three in WLM.

3. H II REGION IDENTIFICATIONS

H II regions were identified on our continuum-subtracted images using the IRAF package HALPHA, which automatically finds the well-separated objects (Phillips 1993). Experimentation showed that prior unsharp masking of the images made it easier for the program to find H II regions in crowded and high-background areas. Diffuse Hα, however, could only be detected and mapped from the untreated subtracted images. Our procedures especially with respect to separation of close and complex H II regions, are described in more detail in Miller & Hodge (1994). Positions for each detected H II region (Table 2) were determined by astrometry with respect to stars listed in the *HST* Guide Star Catalog (Lasker et al. 1990), and should be accurate at the 2″ level.

For WLM we detected 21 separate H II regions (Fig. 1), most of which are also visible in the Hα image published by Hunter (1993). H II region No. 19 should be considered as doubtful, since it has a very faint surface brightness and could be a CCD flat-fielding artifact. The number of H II regions is consistent with the intrinsic size and distance of the galaxy, considering the fact that our CCD frame did not reach very faint levels (§ 4) because of an unusually bright sky caused by proximity of the Moon.

For EGB 0427+63 we detected 25 H II regions (Fig. 2). They are concentrated in two well-separated regions of the galaxy. Their number is consistent with the assumed distance and intrinsic size of the galaxy.

For UGC A86 we detected 115 H II regions (Fig. 3). They are spread out over the entire area of the galaxy, with two conspicuous concentrations that correspond to the two stellar concentrations noted by Saha & Hoessel (1991). The fact that there are H II regions occupying the intervening space (and areas beyond) argues circumstantially against the possibility that UGC A86 is an optical pair of two galaxies. The large number of H II regions (compared to the other galaxies in this survey) suggests that UGC A86 is relatively large intrinsically, which is consistent with our assumption that it lies beyond the Local Group.

We detected no H II regions in LGS 3. The H-R diagram indicates that there are probably no massive main-sequence stars in the system, and thus nothing to excite the H I gas that is present (Lo et al. 1993). The upper limit to the flux of a reasonably compact H II region that we could detect on the frame is approximately 2×10^{15} ergs cm^{-2} s^{-1}. Hunter, Hawley, & Gallagher (1993) also reported a null result.

4. Hα LUMINOSITY FUNCTIONS

We measured the Hα luminosities of the H II regions on the continuum-subtracted images, with borders set at a flux level of approximately 2×10^{-17} ergs s^{-1} cm^{-2} arcsec^{-2}. Table 2 gives the derived fluxes for each H II region detected. The tabulated values include contamination by [N II] lines. The [N II]/H ratio is known only for the brightest H II regions (see § 6); it is small because of the low heavy element abundances found, and thus we expect the [N II] contribution to be small (less than 5%) for all the H II regions. We estimate that this factor, together with photometric uncertainties, leads to a total of approximately 10% uncertainty in the derived fluxes.

Hα luminosities were calculated using the above-cited adopted distances and foreground reddenings, together with the relation $A_{H\alpha} = 2.32E(B-V)$. For these calculations, we corrected for the [N II] contamination, adopting the mean values obtained from our spectra of the bright H II regions in each galaxy. Internal reddening could be determined from the Balmer decrement measured for these H II regions (§ 6). We adopted the mean of the measured values for all the H II regions in each galaxy.

Luminosity functions for the H II regions in each galaxy are shown in Figure 4. The data are displayed as differential luminosity functions with logarithmic bins and with the number of H II regions in each bin being divided by the bin width.

The luminosity function for the H II regions of UGC A86 has a slope, a, of -1.9 ± 0.1 when fitted by least-squares to a power-law relation of the form

$$N(L) = AL^a\, dL\ ,$$

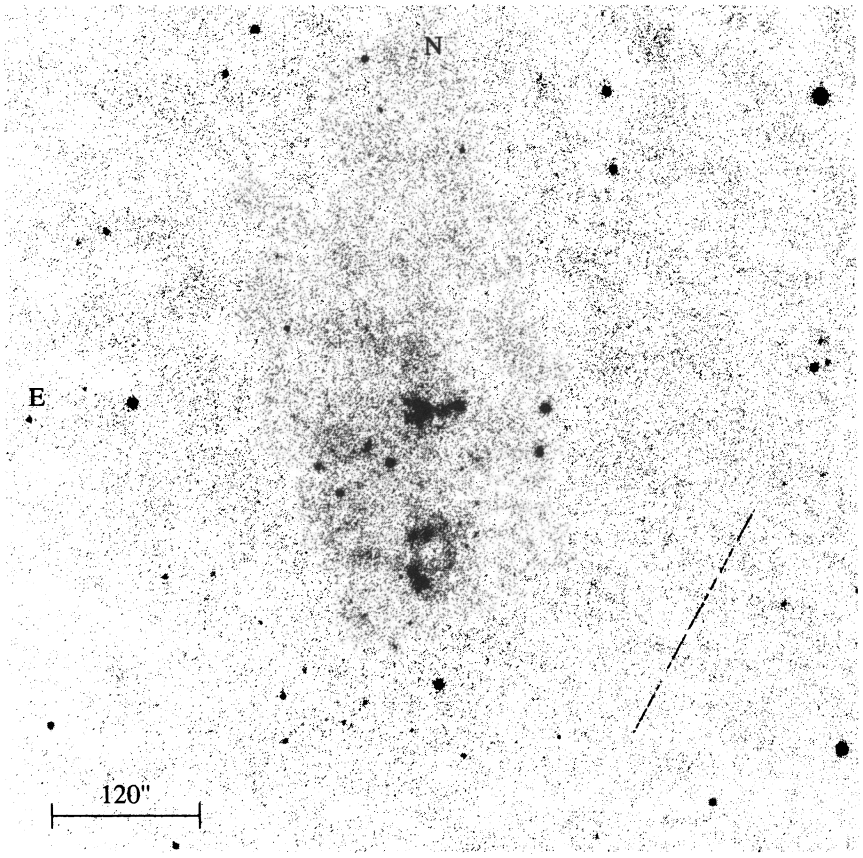

FIG. 1*a*

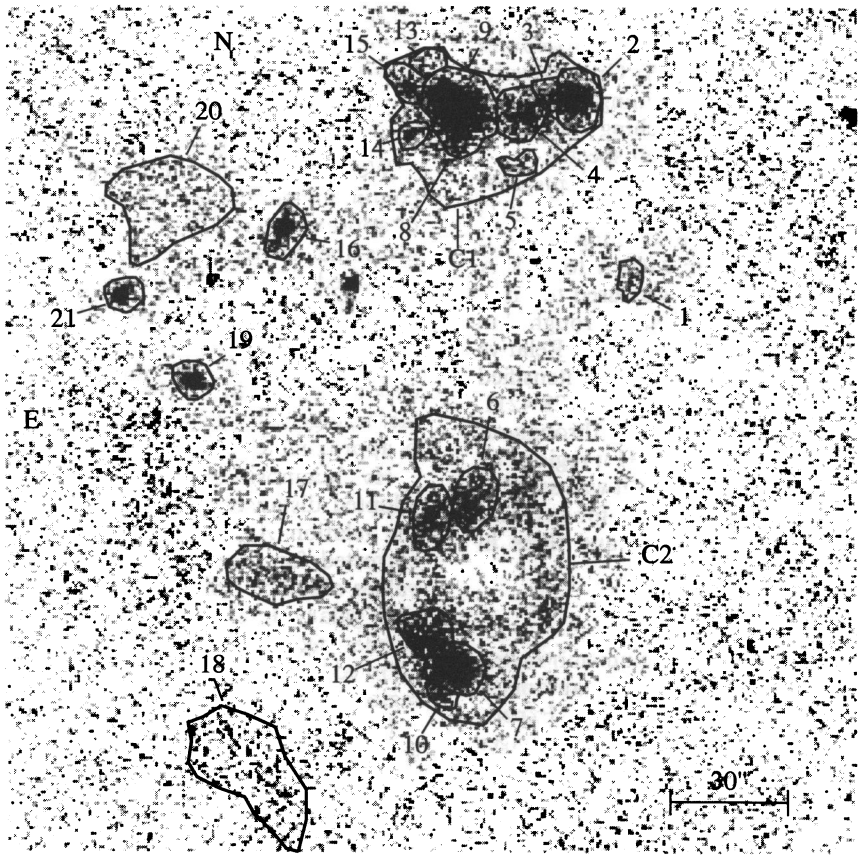

FIG. 1*b*

FIG. 1.—The WLM dwarf: (*a*) in an unsubtracted Hα image and (*b*) in a continuum-subtracted image with the H II regions identified (KPNO 0.9 m CCD images)

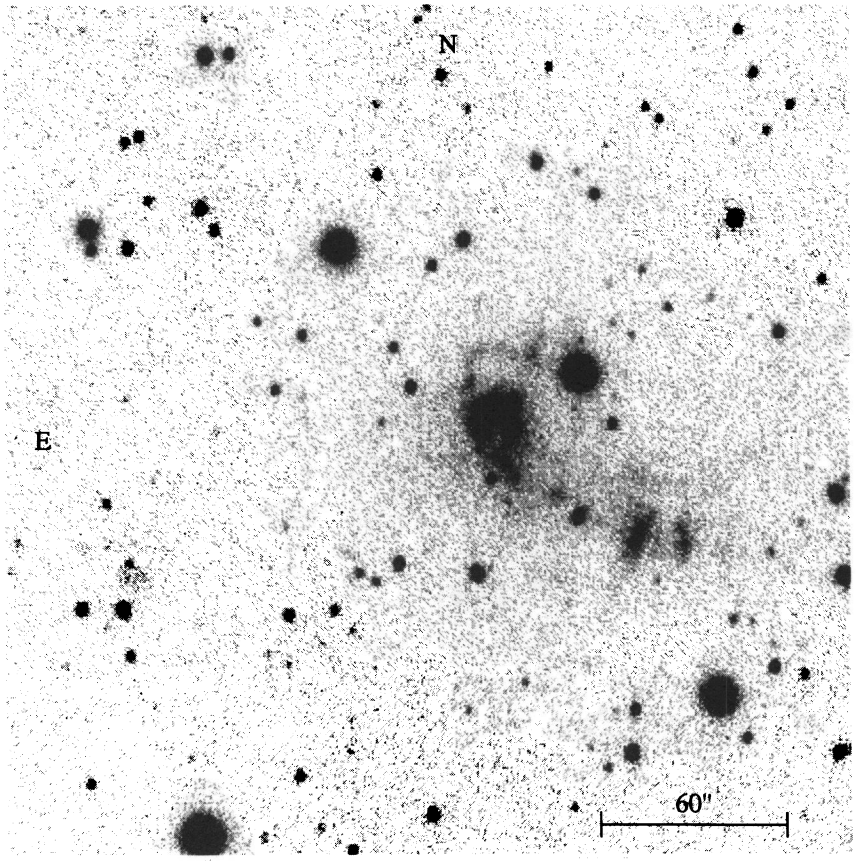

FIG. 2*a*

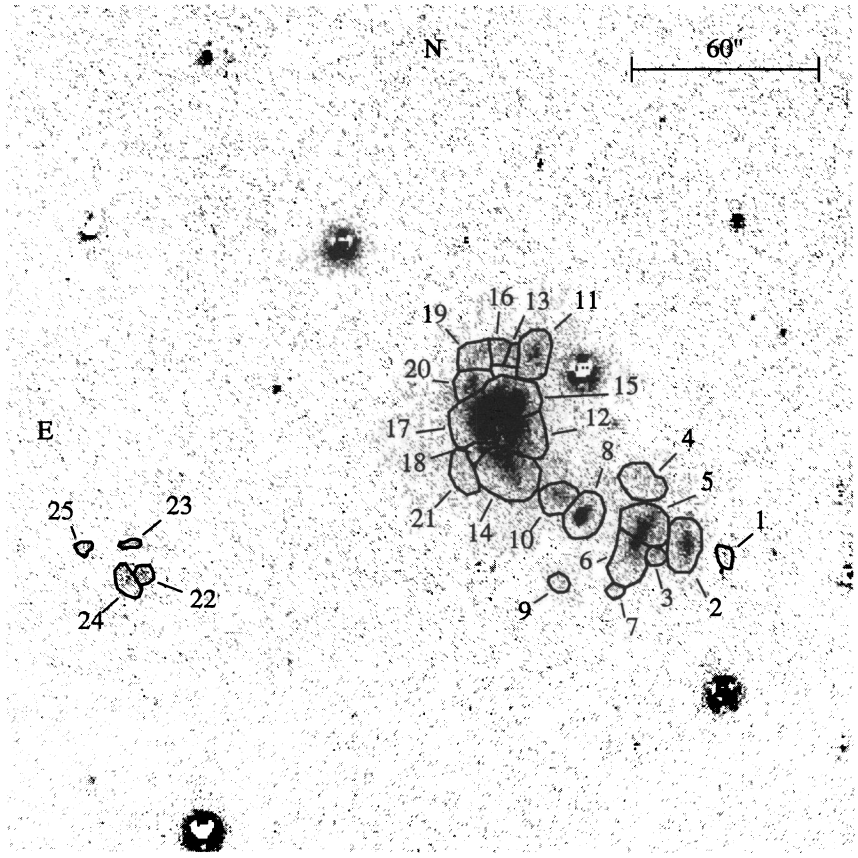

FIG. 2*b*

FIG. 2.—The EGB 0427 + 63 dwarf: (*a*) in an unsubtracted Hα image and (*b*) in a continuum-subtracted image with the H II regions identified (KPNO 0.9 m CCD images).

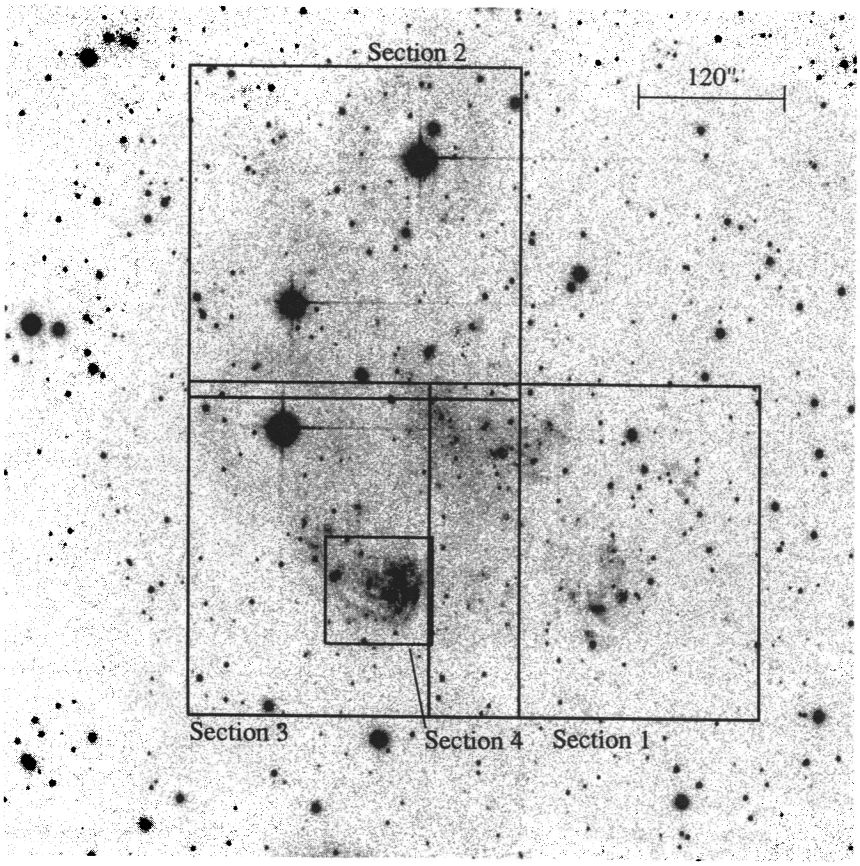

FIG. 3*a*

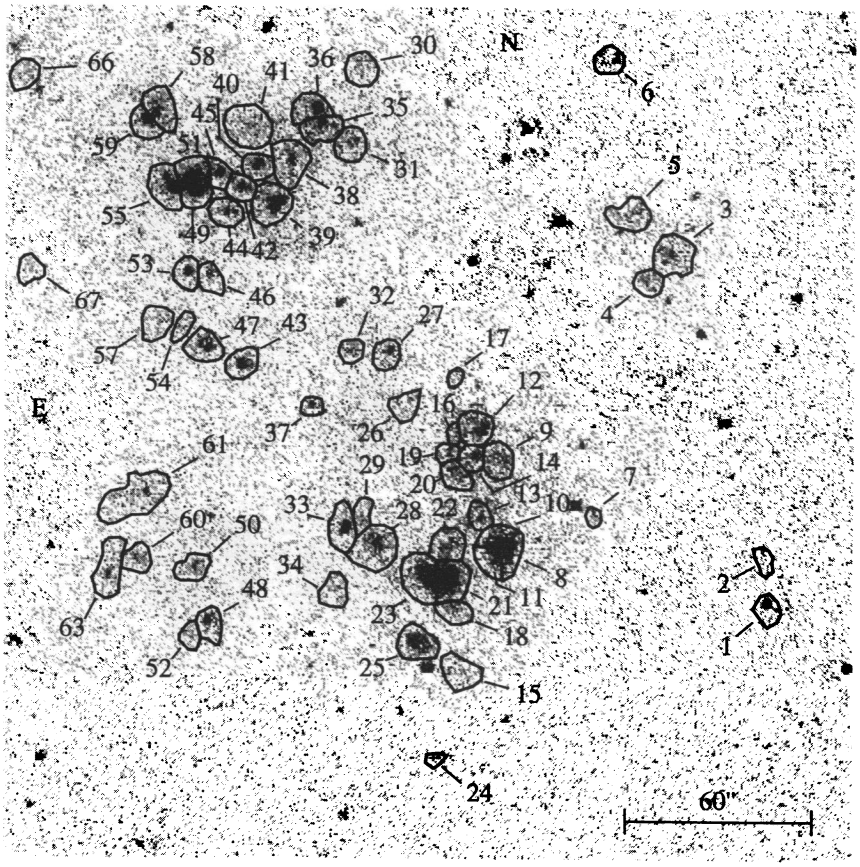

FIG. 3*b*

FIG. 3.—UGC A86: (*a*) in an unsubtracted Hα image with the charted regions identified and (*b*)–(*e*) in continuum-subtracted images of Sections 1–4, respectively, with the H II regions identified (KPNO 0.9 m CCD images).

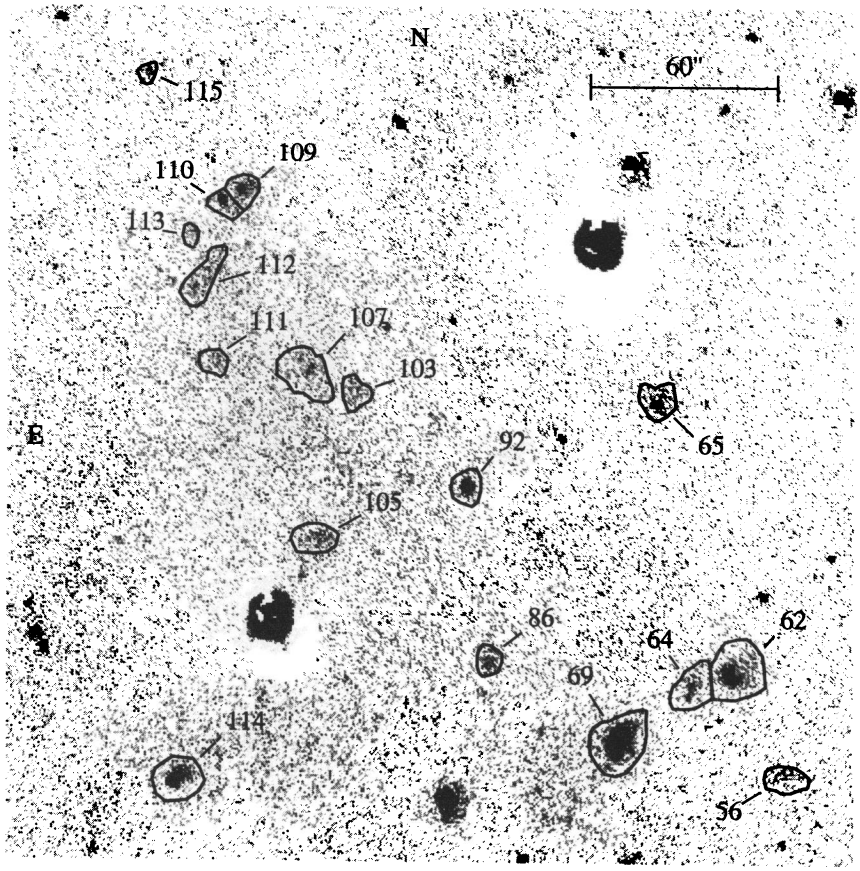

FIG. 3*c*

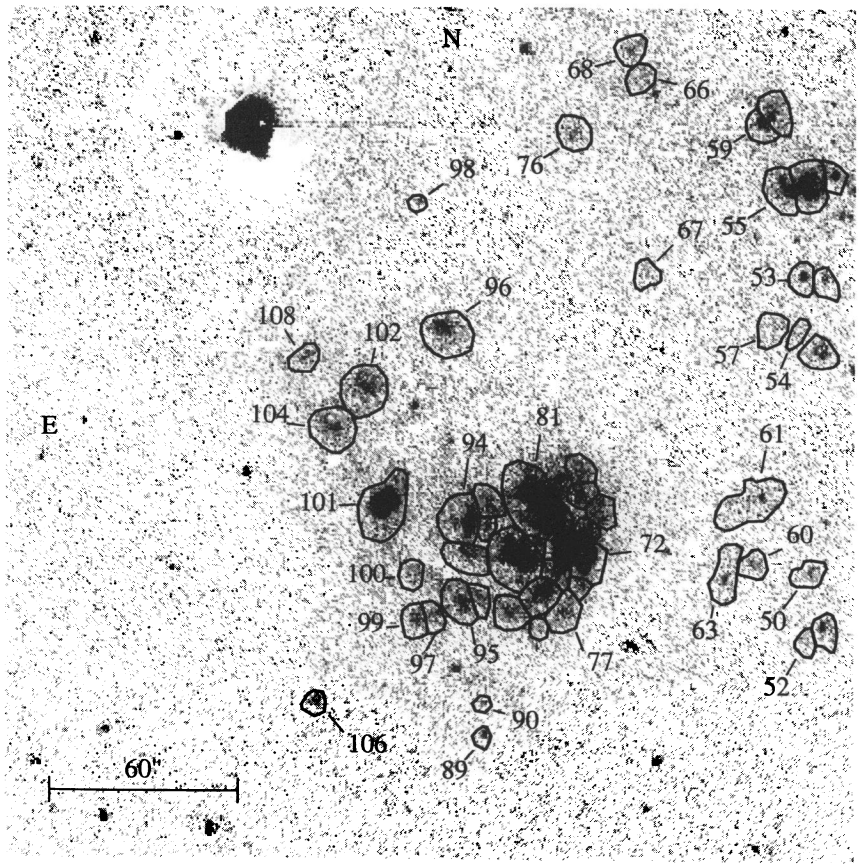

FIG. 3*d*

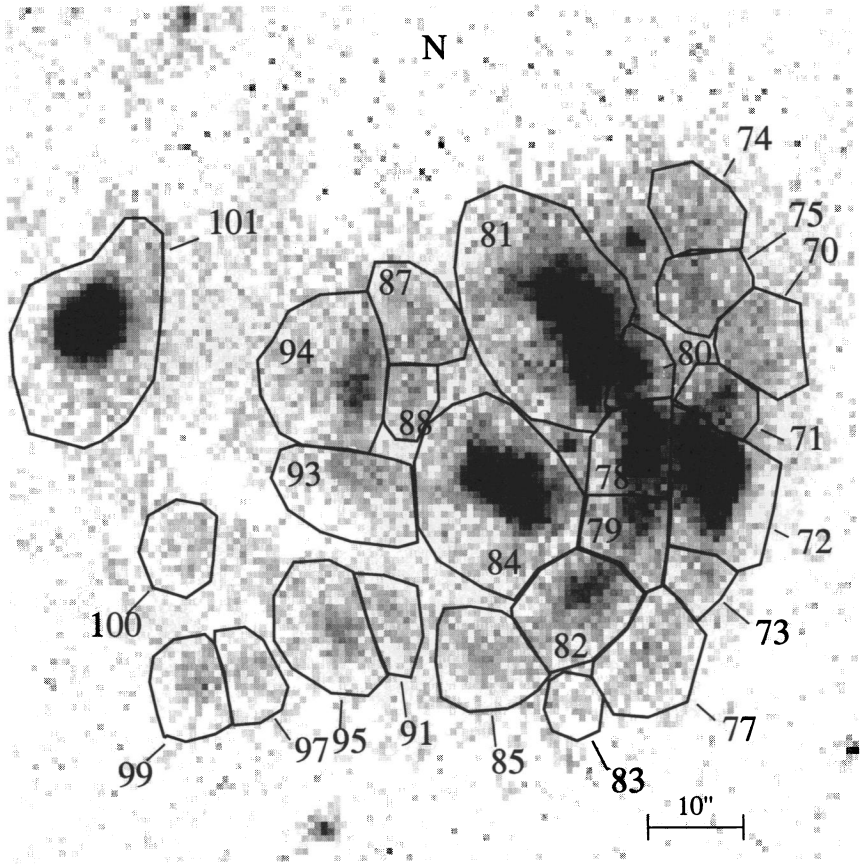

FIG. 3e

which usually provides a good fit for normal galaxies (Kennicutt et al. 1989). That for EGB 0427+63 has a slope of -1.1 ± 0.5. The curve for WLM has only four points because of the bright sky at the time of the exposure. These points define a slope of $a = -1.2 \pm 0.3$. The derived slopes (Table 3) are in reasonable agreement with those for other dwarf irregular galaxies (Kennicutt, Edgar, & Hodge 1989).

5. SIZES AND SIZE DISTRIBUTIONS

The diameters of H II regions are found to follow an exponential distribution reasonably well (van den Burgh 1981), with a slope, D_0, that is fairly independent of the photometric level to which the diameters are measured (see Hodge, Lee, & Kennicutt 1989 for tests made on NGC 6822 H II regions). For the present sample we have determined sizes and size distributions for the H II regions using a parameter that we call the "effective diameter," which is defined as $D = 2(A/\pi)^{1/2}$, where A is the measured area of the H II regions within a uniform isophote level of 2×10^{-17} ergs s^{-1} cm^{-2}. Cumulative diameter distributions are plotted in Figure 5. The slopes for unweighted least-squares fits to the linear portion of the curves are given in Table 3. These "characteristic sizes" are in the normal range for low-luminosity irregular galaxies (e.g., Hodge 1983).

6. ABUNDANCES

The emission-line spectra have been used to determine elemental abundances (primarily oxygen) and reddenings. Table 4 lists the lines detected and their properties. The Balmer lines have been corrected for underlying stellar absorption by adding 2 Å equivalent width. Electron densities could be deter mined for spectra that showed [S II] 6717/6731 lines, but in most cases we had only upper limits to the strengths of these lines. The values calculated agreed reasonably well with the canonical value of 100 cm^{-3}, which we therefore adopted in all calculations. The WLM H II regions were bright enough for us to be able to detect [O III] 4363 (e.g., see Fig. 6) so that we could directly measure the temperatures in the O^{++} regions, which averaged $1.65 \pm 0.15 \times 10^4$ K. For UGC A86, we assumed a temperature of 1.2×10^4 K, and for EGB 0427+66 we used 1.5×10^4 K. We followed the arguments of Skillman & Kennicutt (1993) regarding the differences in temperature between the O^+ and O^{++} zones in our calculations.

For the WLM H II regions, which had measured temperatures, we have calculated oxygen abundances using the direct method (e.g., Osterbrock 1989; Skillman & Kennicutt 1993). Ionic and total oxygen abundances are given in Table 5. For the other H II regions, the "bright line" method was employed (Edmunds & Pagel 1984; Skillman 1989), using the lower branch abundances, arguing for that choice on the basis of the low absolute magnitudes of these dwarf galaxies (see Miller 1994 for further details). The derived abundance values have true uncertainties that we estimate to be approximately 50%, based on the spread in the R23 relation (Skillman 1989). Results for all H II regions, as listed in Table 5, indicate that the three galaxies are all low heavy element objects, with oxygen abundances averaging about 7% solar.

The only previous measurement of abundances in these galaxies is for WLM (Skillman et al. 1989), in which two H II regions were observed (their No. 1 apparently responds to our

TABLE 2

H II Regions in Local Group Dwarf Galaxies

Number	Coordinate (1950) α	δ	Flux ($\times 10^{-15}$) erg cm^{-2} s^{-1}	Diameter (arcsec)	Morphology Class
WLM					
HM 1	$23^h59^m19^s.5$	-15°44′ 20″	9.82	6.4	f
HM 2	23 59 20.5	-15 43 33	52.74	11.1	b
HM 3	23 59 21.0	-15 43 34	13.68	6.1	f
HM 4	23 59 21.4	-15 43 37	40.72	10.6	b
HM 5	23 59 21.5	-15 43 52	9.22	6.1	f
HM 6	23 59 22.4	-15 45 20	45.54	10.6	b
HM 7	23 59 22.6	-15 46 03	159.23	11.3	b
HM 8	23 59 22.6	-15 43 42	54.55	10.2	b
HM 9	23 59 22.8	-15 43 34	107.79	12.6	b
HM 10	23 59 22.9	-15 46 10	10.86	5.4	f
HM 11	23 59 23.1	-15 45 22	37.54	10.0	b
HM 12	23 59 23.3	-15 45 55	45.86	10.0	f
HM 13	23 59 23.3	-15 43 25	9.44	6.3	f
HM 14	23 59 23.6	-15 43 44	10.29	5.8	f
HM 15	23 59 23.6	-15 43 30	19.88	7.6	f
HM 16	23 59 25.8	-15 44 08	32.89	9.1	b
HM 17	23 59 25.9	-15 45 39	52.37	14.9	d
HM 18	23 59 26.5	-15 46 32	63.26	22.0	d
HM 19	23 59 27.4	-15 44 48	23.63	8.0	b
HM 20	23 59 27.9	-15 44 04	75.25	21.0	d
HM 21	23 59 28.7	-15 44 26	21.32	7.4	b
EGB 0427+63					
HM 1	$04^h27^m19^s.7$	+63°29′ 59″	.84	4.9	f
HM 2	04 27 21.6	+63 30 02	11.34	11.3	f
HM 3	04 27 23.1	+63 29 59	1.53	5.1	f
HM 4	04 27 23.6	+63 30 22	5.31	10.2	f
HM 5	04 27 23.8	+63 30 08	15.13	11.5	f
HM 6	04 27 24.2	+63 30 02	11.19	11.4	f
HM 7	04 27 25.3	+63 29 48	.95	4.2	f
HM 8	04 27 26.9	+63 30 11	13.99	10.8	b
HM 9	04 27 27.7	+63 29 49	1.13	5.1	f
HM 10	04 27 28.0	+63 30 18	7.10	8.9	f
HM 11	04 27 29.2	+63 31 03	10.77	10.7	f
HM 12	04 27 29.8	+63 30 40	25.28	11.5	b
HM 13	04 27 30.0	+63 31 03	1.55	4.6	f
HM 14	04 27 30.2	+63 30 28	27.04	14.6	f
HM 15	04 27 30.5	+63 30 47	52.34	13.6	b
HM 16	04 27 30.7	+63 31 05	2.54	6.1	f
HM 17	04 27 31.4	+63 30 44	40.16	12.8	b
HM 18	04 27 31.7	+63 30 33	3.93	5.4	f
HM 19	04 27 31.8	+63 31 05	4.82	8.5	f
HM 20	04 27 32.1	+63 30 54	6.61	8.2	f
HM 21	04 27 32.5	+63 30 25	4.14	8.7	f
HM 22	04 27 48.1	+63 29 53	1.43	5.0	f
HM 23	04 27 48.7	+63 30 03	.60	3.3	f
HM 24	04 27 48.9	+63 29 50	2.77	7.0	f
HM 25	04 27 50.9	+63 30 01	.78	3.8	f
UGC-A 86					
HM 1	$03^h54^m20^s.2$	+66°57′ 21″	2.62	6.9	f
HM 2	03 54 20.5	+66 57 38	1.32	5.7	f
HM 3	03 54 25.6	+66 59 16	7.20	10.7	f
HM 4	03 54 26.9	+66 59 08	2.93	7.0	f
HM 5	03 54 27.9	+66 59 29	5.38	9.4	f
HM 6	03 54 29.3	+67 00 18	3.08	7.2	f
HM 7	03 54 29.9	+66 57 51	1.14	4.5	f
HM 8	03 54 34.7	+66 57 40	7.77	7.5	f
HM 9	03 54 34.8	+66 58 08	6.15	8.8	f
HM 10	03 54 35.1	+66 57 41	8.76	7.7	b
HM 11	03 54 35.3	+66 57 38	6.26	7.5	b
HM 12	03 54 36.2	+66 58 18	7.72	8.9	f
HM 13	03 54 36.2	+66 57 49	3.59	6.7	f

TABLE 2—*Continued*

Number	Coordinate (1950) α	δ	Flux ($\times 10^{-15}$) erg cm^{-2} s^{-1}	Diameter (arcsec)	Morphology Class
HM 14	03 54 36.5	+66 58 09	4.27	6.7	f
HM 15	03 54 37.3	+66 56 60	3.76	9.2	f
HM 16	03 54 37.5	+66 58 17	1.35	4.3	f
HM 17	03 54 37.5	+66 58 37	.95	4.4	f
HM 18	03 54 37.7	+66 57 21	3.79	7.4	f
HM 19	03 54 37.8	+66 58 05	4.48	7.5	f
HM 20	03 54 37.9	+66 58 10	2.03	5.4	f
HM 21	03 54 38.0	+66 57 30	18.62	9.8	b
HM 22	03 54 38.2	+66 57 39	6.46	9.0	f
HM 23	03 54 38.8	+66 57 29	15.34	11.0	b
HM 24	03 54 38.8	+66 56 33	.68	4.1	f
HM 25	03 54 39.9	+66 57 10	9.11	9.6	b
HM 26	03 54 40.0	+66 58 27	2.44	7.5	f
HM 27	03 54 41.3	+66 58 44	3.58	7.5	b
HM 28	03 54 42.0	+66 57 41	9.39	11.7	f
HM 29	03 54 42.9	+66 57 48	2.67	6.6	f
HM 30	03 54 43.1	+67 00 18	4.18	8.4	f
HM 31	03 54 43.3	+66 59 53	5.23	8.5	f
HM 32	03 54 43.3	+66 58 44	2.43	6.3	f
HM 33	03 54 43.8	+66 57 46	6.50	9.3	b
HM 34	03 54 44.3	+66 57 26	2.81	7.7	f
HM 35	03 54 45.1	+66 59 58	8.22	8.6	b
HM 36	03 54 45.3	+67 00 03	8.07	8.4	b
HM 37	03 54 45.6	+66 58 26	1.72	5.4	f
HM 38	03 54 46.8	+66 59 47	8.87	10.6	b
HM 39	03 54 47.5	+66 59 33	11.71	10.5	b
HM 40	03 54 48.6	+66 59 46	5.30	7.5	b
HM 41	03 54 48.9	+66 59 58	8.82	11.4	f
HM 42	03 54 49.5	+66 59 38	5.09	7.3	f
HM 43	03 54 49.5	+66 58 40	5.15	8.1	b
HM 44	03 54 50.3	+66 59 30	4.23	8.0	f
HM 45	03 54 50.7	+66 59 42	4.66	6.7	b
HM 46	03 54 51.3	+66 59 09	2.92	7.0	f
HM 47	03 54 51.3	+66 58 46	5.89	8.9	f
HM 48	03 54 51.4	+66 57 16	4.06	7.5	b
HM 49	03 54 52.1	+66 59 37	7.55	6.9	b
HM 50	03 54 52.1	+66 57 33	3.28	7.8	f
HM 51	03 54 52.2	+66 59 40	18.98	8.9	b
HM 52	03 54 52.3	+66 57 12	1.66	5.9	f
HM 53	03 54 52.5	+66 59 10	4.00	7.3	b
HM 54	03 54 52.9	+66 58 52	1.55	5.8	f
HM 55	03 54 53.2	+66 59 38	12.04	9.9	b
HM 56	03 54 53.4	+67 00 51	4.49	8.8	f
HM 57	03 54 54.0	+66 58 54	3.17	8.4	f
HM 58	03 54 54.2	+67 00 02	8.91	9.2	b
HM 59	03 54 54.7	+66 59 60	5.96	7.3	b
HM 60	03 54 55.3	+66 57 36	3.14	7.2	f
HM 61	03 54 55.5	+66 57 57	10.92	13.6	d
HM 62	03 54 56.4	+67 01 22	19.34	14.7	b
HM 63	03 54 56.9	+66 57 31	5.96	10.3	d
HM 64	03 54 58.4	+67 01 20	6.77	10.9	f
HM 65	03 55 00.6	+67 02 50	5.48	9.2	f
HM 66	03 55 01.1	+67 00 13	3.98	7.4	f
HM 67	03 55 01.2	+66 59 11	2.10	6.8	f
HM 68	03 55 02.0	+67 00 23	4.16	7.7	f
HM 69	03 55 02.4	+67 01 03	29.20	14.9	b
HM 70	03 55 03.7	+66 57 50	9.67	7.9	f
HM 71	03 55 04.4	+66 57 46	8.15	5.9	b
HM 72	03 55 04.6	+66 57 39	54.12	10.6	b
HM 73	03 55 04.7	+66 57 30	3.55	5.4	f
HM 74	03 55 04.8	+66 58 06	7.96	7.6	f
HM 75	03 55 04.9	+66 57 59	8.85	7.2	f

TABLE 2—*Continued*

Number	Coordinate (1950) α	Coordinate (1950) δ	Flux ($\times 10^{-15}$) erg cm^{-2} s^{-1}	Diameter (arcsec)	Morphology Class
HM 76	03 55 05.3	+66 59 56	4.86	8.9	f
HM 77	03 55 05.8	+66 57 20	8.18	9.1	f
HM 78	03 55 05.8	+66 57 43	29.94	7.8	b
HM 79	03 55 05.9	+66 57 36	12.37	7.3	b
HM 80	03 55 06.2	+66 57 50	12.33	5.9	b
HM 81	03 55 06.8	+66 57 54	99.30	16.2	b
HM 82	03 55 06.9	+66 57 27	15.45	9.4	b
HM 83	03 55 07.2	+66 57 15	1.95	5.2	f
HM 84	03 55 08.4	+66 57 39	54.17	14.5	b
HM 85	03 55 08.8	+66 57 21	8.55	8.9	f
HM 86	03 55 09.9	+67 01 27	3.17	7.1	f
HM 87	03 55 09.9	+66 57 54	7.91	8.1	f
HM 88	03 55 10.0	+66 57 48	3.77	5.5	f
HM 89	03 55 10.2	+66 56 41	1.69	4.8	f
HM 90	03 55 10.2	+66 56 52	.98	4.3	f
HM 91	03 55 10.4	+66 57 25	4.00	6.3	f
HM 92	03 55 11.0	+67 02 24	9.17	8.4	b
HM 93	03 55 11.0	+66 57 39	9.64	9.9	f
HM 94	03 55 11.1	+66 57 48	19.49	11.9	f
HM 95	03 55 11.4	+66 57 23	10.86	9.6	f
HM 96	03 55 12.5	+66 58 54	13.92	12.5	b
HM 97	03 55 12.9	+66 57 20	3.50	6.5	f
HM 98	03 55 13.8	+66 59 34	1.02	4.4	f
HM 99	03 55 13.9	+66 57 18	5.22	7.6	f
HM 100	03 55 13.9	+66 57 33	4.03	7.0	f
HM 101	03 55 15.7	+66 57 56	58.75	14.5	b
HM 102	03 55 16.8	+66 58 34	16.29	12.8	f
HM 103	03 55 17.1	+67 02 55	3.30	7.7	f
HM 104	03 55 18.4	+66 58 20	12.32	11.6	f
HM 105	03 55 19.2	+67 02 07	5.22	9.7	f
HM 106	03 55 19.5	+66 56 52	2.37	6.0	f
HM 107	03 55 19.8	+67 03 01	8.39	12.9	d
HM 108	03 55 20.1	+66 58 44	3.80	7.3	f
HM 109	03 55 23.7	+67 03 59	6.30	8.1	b
HM 110	03 55 24.7	+67 03 55	5.00	7.2	b
HM 111	03 55 25.0	+67 03 05	2.31	6.8	f
HM 112	03 55 25.5	+67 03 31	5.98	10.2	d
HM 113	03 55 26.2	+67 03 45	1.28	4.8	f
HM 114	03 55 27.2	+67 00 48	9.32	11.9	b
HM 115	03 55 28.8	+67 04 38	1.37	4.7	f

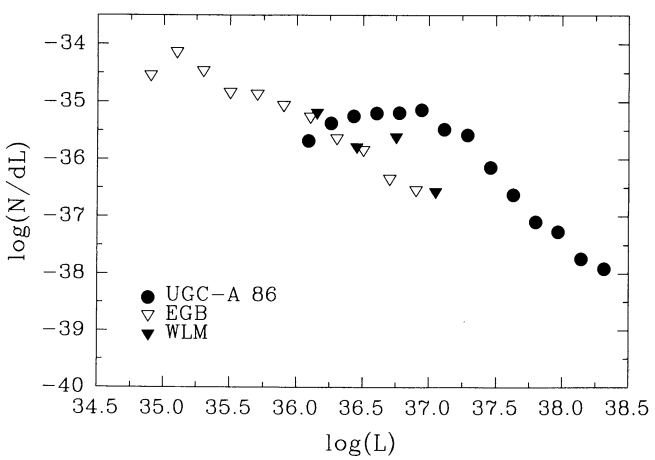

FIG. 4.—Hα luminosity functions for three galaxies. Luminosities are in units of ergs s^{-1}. Note that if our assumed distances to UGC A86 and EGB 0427+63 are wrong, their curves in this and the following figure will shift laterally.

No. 9). Their values for oxygen abundances (Table 5) agree within the errors with ours.

Table 6 lists the derived values for $c(\mathrm{H}\beta)$, the logarithmic extinction at Hβ. We have converted these to reddening values using the relation

$$E(B-V) = c(\mathrm{H}\beta)/0.4(R + 0.53)$$

(see Howarth 1983) and a value of R of 3.1. These values are about equal to or larger than the adopted values for foreground reddening, indicating the presence of some internal reddening in the galaxies and their H II regions. For UGC A86 the difference is negative, suggesting that there is very little internal reddening. This result is contrary to the suggestion of

TABLE 3

SCALE PARAMETERS

Galaxy	a	D_0 (pc)
WLM	-1.2 ± 0.3	34 ± 10
EGB 0427+63.....	-1.1 ± 0.5	20 ± 6
UGC A86	-1.9 ± 0.1	40 ± 4

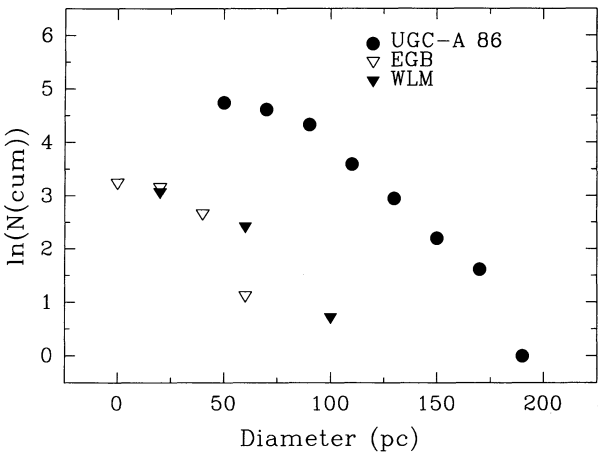

FIG. 5.—Size distributions for the three galaxies

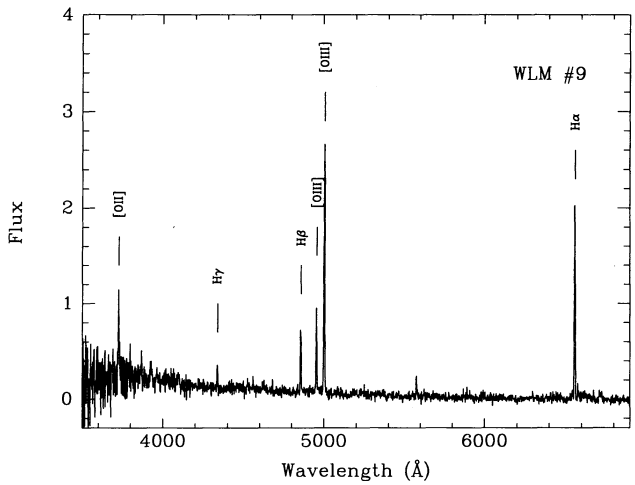

FIG. 6.—Spectrum of H II region No. 9 in WLM with some of the lines identified (KPNO 2.1 m telescope).

TABLE 4

LINE RATIOS

Line	WLM No. 7	WLM No. 9	EGB No. 15	EGB No. 17	UGC A86 No. 81	UGC A86 No. 101
3727 [O II]	1.45 ± 0.26	1.04 ± 0.23	0.39 ± 0.85	1.75 ± 1.53	1.73 ± 1.27	2.10 ± 1.54
3868 [Ne III]	0.39 ± 0.07	0.32 ± 0.10	...	...	...	...
3889 H8 + He I	0.26 ± 0.05	...	...	...	...	...
3968 H7 + [Ne III]	0.28 ± 0.05	0.18 ± 0.06	...	...	...	...
4026 He I	...	...	0.41 ± 0.29	0.55 ± 0.39	...	...
4101 Hδ	0.29 ± 0.05	0.28 ± 0.09	...	...	...	...
4340 Hγ	0.51 ± 0.07	0.45 ± 0.09	...	...	0.48 ± 0.19	0.63 ± 0.25
4363 [O III]	0.09 ± 0.01	0.05 ± 0.06	...	...	...	...
4471 He I	0.05 ± 0.01	...	...	...	...	...
4861 Hβ	1.00 ± 0.13	1.00 ± 0.14	1.00 ± 0.23	1.00 ± 0.21	1.00 ± 0.14	1.00 ± 0.14
4959 [O III]	1.23 ± 0.16	1.50 ± 0.21	1.15 ± 0.25	1.35 ± 0.29	1.42 ± 0.22	0.96 ± 0.15
5007 [O III]	3.70 ± 0.48	4.32 ± 0.58	3.35 ± 0.75	4.35 ± 0.98	4.37 ± 0.75	3.02 ± 0.51
5876 He I	0.11 ± 0.02	0.07 ± 0.03	0.15 ± 00.12	0.18 ± 0.14	0.14 ± 0.09	0.16 ± 0.10
6312 [S III]	...	...	...	...	0.02 ± 0.02	0.05 ± 0.05
6563 Hα	2.42 ± 2.47	2.97 ± 0.59	2.82 ± 2.55	2.87 ± 3.00	3.00 ± 2.68	2.92 ± 2.61
6584 [N II]	0.04 ± 0.01	0.13 ± 0.04	0.07 ± 0.07	0.03 ± 0.04	0.09 ± 0.09	0.10 ± 0.09
6678 He I	...	0.04 ± 0.02	...	...	0.04 ± 0.04	0.04 ± 0.04
6717 [S II]	0.10 ± 0.02	0.18 ± 0.05	0.12 ± 0.12	0.10 ± 0.12	0.15 ± 0.15	0.16 ± 0.16
6731 [S II]	0.08 ± 0.02	0.16 ± 0.04	0.07 ± 0.07	0.06 ± 0.07	0.11 ± 0.11	0.12 ± 0.12
7135 [Ar III]	0.06 ± 0.01	0.09 ± 0.03	0.04 ± 0.05	0.11 ± 0.14	0.08 ± 0.09	0.06 ± 0.07
c (Hβ)	0.00 ± 0.16	0.29 ± 0.28	1.21 ± 0.91	1.43 ± 1.05	1.19 ± 0.57	0.52 ± 0.57
EW (Hβ)	377	40.5	112	60.3	73.1	223
F (Hβ) × 10^{-15}	15.7	7.24	0.78	0.61	2.93	3.22
log [O II]/[O III]	−0.53 ± 0.09	−0.75 ± 0.11	01.06 ± 0.95	00.51 ± 0.35	−0.52 ± 0.32	−0.28 ± 0.32
log (R23)	0.80 ± 0.04	0.84 ± 0.04	0.73 ± 0.14	0.87 ± 0.14	0.88 ± 0.09	0.78 ± 0.12
log [O III]/[N II]	2.05 ± 0.10	1.66 ± 0.13	1.82 ± 0.44	2.23 ± 0.52	1.80 ± 0.40	1.60 ± 0.40
log [N II]/[O II]	−1.52 ± 0.12	−0.91 ± 0.16	−0.78 ± 1.04	−1.71 ± 0.64	−1.27 ± 0.51	−1.32 ± 0.51

TABLE 5

ABUNDANCES OF H II REGIONS

H II Region	O/H (× 10^5)	N/O (× 100)	Ne II/H (× 10^6)	S II/H (× 10^7)	Ar III/H (× 10^7)	O/H (× 10^5)[a]
WLM No. 7	5.2 ± 0.8	2.5 ± 0.8	7 ± 2	1.7 ± 0.4	2.2 ± 0.6	6 ± 3
WLM No. 9	6.5 ± 1.1	10 ± 5	7.3 ± 2.5	3.7 ± 1.0	3.9 ± 1.4	...
EGB No. 15	5(+4/−2)	<3	...	<4	<11	...
EGB No. 17	4(+2/−1)	<12	...	<3	<5	...
UGC A86 No. 81	7 ± 2	<8	...	<6	<5	...
UGC A86 No. 101	6 ± 2	<12	...	<6	<6	...

[a] Skillman et al. 1989.

TABLE 6

REDDENINGS

Galaxy	Mean $c(H\beta)$	Mean $E(B-V)$	Adopted Foreground $E(B-V)$
WLM	0.14 ± 0.14	0.10 ± 0.10	0.02
EGB 0427+63.....	1.32 ± 0.11	0.90 ± 0.08	0.25
UGC A86	0.85 ± 0.33	0.59 ± 0.23	0.65

TABLE 7

STAR FORMATION RATES AND FORMATION TIMES

Galaxy	log L (Hα) (ergs s^{-1})	Star Formation Rate ($M_\odot$ yr^{-1})	τ_{form} (Gyr)
WLM	1.2×10^{38}	0.0011	150
EGB 0427+63.....	1.3×10^{38}	0.0012	...
UGC A86	1.6×10^{39}	0.014	7
LGS 3	0	0	∞

Richter et al. (1991), who suggest that the star-forming regions of the galaxy might be heavily reddened, as indicated by the presence of the infrared source IRAS 3550+6557 in the field. Apparently the source, if it is connected with UGC A86, is not involved with the H II regions for which we measured reddenings.

7. TOTAL STAR FORMATION RATES

To gain an idea of the level of star-forming activity in the galaxies discussed here, we have calculated total star formation rates using the precepts given by Kennicutt (1983), which assume a modified Salpeter IMF. Table 7 lists these data, which are based on the sum of the fluxes of the H II regions identified in Table 1. This total ignores any diffuse Hα emission that may be present, which may introduce only a small error, according to comparisons for similar galaxies (Miller & Hodge 1994). The range of current star formation rates is from zero for LGS 3 to 0.014 $M_\odot$ yr^{-1} for UGC A86.

Another informative parameter is the formation timescale that is determined by comparing the present star formation rate with the total rate that would be needed to form all the galaxy's stars (Kennicutt 1983). We have defined this in terms of the timescale, τ_{form}, calculated by using the total blue magnitude as a measure of the total stellar content and by assuming that $M/L = 2$ in solar units for determining the total stellar mass; with poor or nonexistent information about the colors of these galaxies, we cannot use galaxy evolution models, as we did for the M81 dwarfs (Miller & Hodge 1994). Table 7 lists values for τ_{form}, which range from infinity (of course) for LGS 3, which is not now forming stars, though it still has H I gas, to 7 Gyr for UGC A86, which has a higher than average level of current activity. WLM, with a value of τ_{form} of 150 Gyr, must be in a relatively quiet phase, a conclusion that agrees with that reached on the basis of model-fitting its color-magnitude diagram (Ferraro et al. 1989). We cannot calculate the formation time for EGB 0427+63 because, with no knowledge of either its apparent magnitude or its distance, there are difficulties in calculating its luminosity.

The figures in Table 7 for the two galaxies with highly uncertain distances (EGB 0427+63 and UGC A86) have to be considered as very tentative, of course. If they are significantly farther than our adopted distances, the star formation rate values will be much larger. The formation timescale will not change, since it is based on the ratio of two luminosities.

In conclusion, we find that these nearby dwarf galaxies represent a full range of star formation histories, from a galaxy that stopped forming stars long ago and that has only a small amount of residual gas (LGS 3), to a galaxy in a higher than average state of star-forming activity (UGC A86).

We are grateful to the National Science Foundation for partial support through grant 92-15821 and to Andrew Dolphin, who helped reduce the spectra and calculated the elemental abundances.

REFERENCES

Ables, H. D. & Ables, P. G. 1977, ApJS, 34, 245
Burstein, D., & Heiles, C. 1984, ApJS, 54, 33
Cook, K. H., & Olszewski, E. 1989, BAAS, 21, 775
de Vaucouleurs, G., de Vaucouleurs, A., Corwin, H., Buta, R., Paturel, G., & Fouque, P. 1991, Third Reference Catalogue of Bright Galaxies (Berlin: Springer-Verlag)
Edmunds, M. G., & Pagel, B. E. J. 1984, MNRAS, 211, 507
Ellis, G. S., Grayson, E. T., & Bond, H. E. 1984, PASP, 96, 283
Ferraro, F. R., Fusi Pecci, F., Tosi, M., & Buonanno, R. 1989, MNRAS, 241, 433
Hodge, P. W. 1983, AJ, 88, 1323
———. 1994, in Dwarf Galaxies, ed. G. Meylan & P. Prugniel (ESO Conf. Proc. No. 49), 501
Hodge, P. W., Lee, M. G., & Kennicutt, R. C. 1989, PASP, 101, 32
Hoessel, J. G., Saha, A., & Danielson, G. E. 1988, PASP, 100, 680
Howarth, I. D. 1983, MNRAS, 203, 301
Hunter, D. A. 1993, AJ, 106, 1797
Hunter, D. A., Hawley, W. N., & Gallagher, J. 1993, AJ, 106, 1797
Karachentsev, I. D., & Tikhonov, N. A. 1993, A&AS, 100, 227
Kennicutt, R. C. 1983, ApJ, 272, 54
Kennicutt, R. C., Edgar, B. K., & Hodge, P. W. 1989, ApJ, 337, 761
Kraan-Korteweg, R. C., & Tammann, G. A. 1979, Astron. Nach., 300, 181
Lasker, B., Sturch, C., McLean, B., Russell, J., Jenkner, H., & Shara, M. 1990, AJ, 99, 2019
Lo, K. Y., Sargent, W. L. W., & Young, K. 1993, AJ, 106, 507
Miller, B. W. 1994, Ph.D. thesis, Univ. of Washington
Miller, B. W., & Hodge, P. 1992, in The Evolution of Galaxies and Their Environment: Proc. Third Teton Summer School on Astrophysics, ed. D. Hollenbach, H. Thronson, & J. Shull (NASA Conf. Publ. 3190), 90
———. 1994, ApJ, 427, 656
Osterbrock, D. E. 1989, Astrophysics of Gaseous Nebulae and Active Galactic Nuclei (Mill Valley: Univ. Sci. Books)
Phillips, A. C. 1993, Ph.D. thesis, Univ. of Washington
Richter, G. M., Schmidt, K. H., Thanert, W., Stavrev, K., & Panov, K. 1991, Astron. Nach., 312, 309
Richter, O., Tammann, G., & Huchtmeier, W. K. 1987, A&A, 171, 33
Saha, A., & Hoessel, J. G. 1991, AJ, 101, 465
Sandage, A. R., & Carlson, G. 1985, AJ, 90, 1019
Schneider, D. P., Gunn, J. E., & Hoessel, J. G. 1983, ApJ, 264, 337
Skillman, E. D. 1989, ApJ, 347, 883
Skillman, E. D., & Kennicutt, R. C. 1993, ApJ, 411, 655
Skillman, E. D., Terlevich, R., & Melnick, J. 1989, MNRAS, 240, 563
Thuan, T. X., & Martin, G. E. 1979, ApJ, 232, L11
van den Bergh, S. 1981, AJ, 86, 1646
———. 1994, AJ, 107, 1328